

Aligned Arrays of Te Nanorods Grown from the Faceted Surfaces of Colloidal GeTe Particles

Hsing-Yu Tuan[†] and Brian A. Korgel*

Department of Chemical Engineering, Texas Materials Institute, Center for Nano- and Molecular Science and Technology, The University of Texas at Austin, Austin, Texas 78712-1062

Received February 22, 2008; Revised Manuscript Received April 12, 2008

ABSTRACT: Reactions carried out with diphenylgermane (DPG) and trioctylphosphine-tellurium (TOP-Te) in supercritical hexane at 460 °C at 13.6 MPa yielded faceted GeTe particles. When octanol was added to the reactions, the GeTe particles formed with arrays of aligned Te nanorods extending off their surfaces. These GeTe/Te heterostructures also formed when other additives such as oleic acid and isoprene were present in the reactions, but the addition of thiols quenched Te nanorod growth. These surfactant additives appear to influence reactant decomposition, deposition, and crystallization kinetics. Careful crystallographic analyses revealed that the Te nanorods extend epitaxially from the faceted GeTe surfaces and that this epitaxial interfacing determined the growth direction of the Te nanorods. This system provides an example of how the lattice mismatch between a deposited material and an underlying substrate can lead to formation of an array of nanowires.

Introduction

Arrays of aligned crystalline nanowires could be useful for a variety of different applications, including field emission sources,^{1–4} light emission sources,⁵ photocatalytic and photovoltaic devices,^{6,7} chemical sensors,⁸ superhydrophobic and electrowetting surfaces,⁹ nanogenerators,^{10,11} nanoelectromechanical resonator arrays,¹² vertical field effect transistors,^{13,14} and structures for biological and macromolecular separations.^{15,16} The realization of these applications relies on the ability to make the arrays efficiently. One way to make an array of nanowires is to use lithography and etching,^{16–18} but these processes can be relatively slow, and in many cases there are limits to the sizes and separation of the posts that can be made this way. In some cases, vertically aligned nanowires can be grown directly from surfaces.^{6,19–23} Vertical growth of nanowires can be induced in part by epitaxial interfacing between the substrate and the nanowire,^{6,19–21} or it can relate to the nanowire growth kinetics.^{22,23} This topic remains an active area of study.

A related subject is branching and heterostructure formation of colloidal nanostructures.^{24,25,29–55} Rational approaches to creating nanostructures with complex geometries and elaborate composition profiles are being developed. In some cases, these unique nanostructures have been utilized in new prototype devices.^{24–28} The synthetic strategies rely on a deep understanding of the relationship between the reaction chemistry and the crystal growth and deposition processes that happen at the nanoscale, and many of these fundamental processes are still being elucidated. Herein we report the formation of colloidal faceted GeTe particles that have arrays of aligned Te nanorods extending from their surfaces and present a detailed study of their crystallographic structure and how it relates to epitaxial growth of Te on the GeTe surface.

Our initial interest in this materials system was in the development of the supercritical fluid–liquid–solid (SFLS) synthesis of GeTe nanowires for use as a phase-change material for information storage.^{56–59} We anticipated that the gold nanocrystal-seeded growth of GeTe nanowires would work, as

others had demonstrated GeTe nanowire growth using gold nanocrystals as seeds in the gas-phase by vapor–liquid–solid (VLS) in a similar temperature range.^{57–59} However, GeTe nanowires did not form under our growth conditions, and instead only submicrometer diameter faceted particles of rhombohedral GeTe were produced. To try to promote nanowire growth, stabilizing molecules were added, such as octanol, oleic acid, isoprene, and hexadecanethiol, which have the potential to bond to Ge in solution and on the crystal surface^{60–62} to slow particle formation. These additives did not prevent particle formation and did not help nanowire growth, but instead gave rise to forests of aligned Te nanowires (in the case of octanol, oleic acid and isoprene) on some of the faceted surfaces of the GeTe particles. Careful examination of the crystallographic details of the nanostructures reveal that the Te nanorods interface epitaxially with the GeTe surface and results in preferred Te growth directions that depend on the lattice spacing of the exposed GeTe surface.

Experimental Details

Synthesis. Anhydrous hexane, octanol, 1-hexadecanethiol, oleic acid, isoprene, trioctylphosphine (TOP), and tellurium powder (99.8%) were purchased from Sigma-Aldrich and diphenylgermane (DPG) was purchased from Gelest. All chemicals were used as received. The reagent solution of 0.75 M elemental Te in trioctylphosphine (TOP-Te) was made in a nitrogen-filled glovebox by dissolving 0.117 g of elemental Te in 3 mL of TOP with vigorously stirring in a sealed 10 mL glassy vial.

All reactions were carried out in a semibatch 10 mL Ti grade-2 reactor (like that described in ref 63) under inert atmosphere. The titanium reactor was opened in a nitrogen-filled glovebox, and a 6.5 cm × 0.8 cm silicon wafer was placed inside to serve as a deposition substrate for collecting the reaction product. The reactor was sealed, removed from the glovebox, and then placed in a preheated brass block. The pressure and precursor injection rate were controlled by a high-pressure liquid chromatography (HPLC) pump that was attached to the reactor. Between the HPLC pump and the reactor is a 6-way valve (Valco) HPLC injection loop for injecting the reactants into the reactor at the reaction temperature and pressure.

The reactor was first filled with anhydrous hexane and heated and pressurized to 3.4 MPa and 460 °C. In the glovebox, 500 μL of hexane with 80 mM DPG and 80 mM TOP-Te were loaded into a syringe. The syringe was removed from the glovebox, and the reaction solution was injected into the HPLC injection loop. In some reactions, octanol,

* Corresponding author: Tel.: (512) 471-5633; fax: (512) 471-7060; e-mail: korgel@mail.che.utexas.edu.

[†] Present address: Department of Chemical Engineering, National Tsing Hua University, Hsinchu 300, Taiwan, Republic of China.

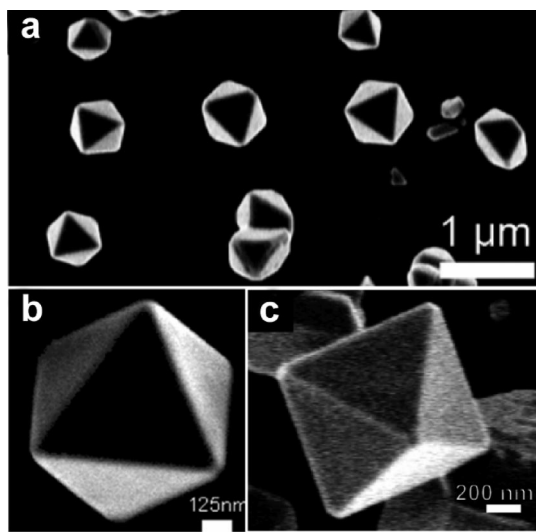


Figure 1. Octahedral GeTe particles produced in reactions between DPG and TOP-Te in supercritical hexane at 460 °C at 13.6 MPa.

oleic acid, isoprene, or 1-dodecanethiol was added to the reactant solution. The reactant solution was then added to the reactor at a flow rate of 4 mL/min. Once the reactants were added, the reactor pressure was increased slightly to 13.6 MPa with additional hexane. The reaction was carried out for 10 min and then the reactor was removed from the

heating block and submerged into an ice bath for 2 min to cool the reactor and quench the reaction. The reactor was then allowed to cool to room temperature before opening. [Note: the reactor needed to be opened very carefully as there was usually some residual pressure in the reactor.] The reaction product was removed from the reactor on the Si substrate. It is a dark gray powder. The product was rinsed with hexane and then stored under nitrogen prior to characterization.

Materials Characterization. The materials were characterized using high-resolution scanning electron microscopy (HRSEM), high-resolution transmission electron microscopy (HRTEM), energy-dispersive X-ray spectroscopy (EDS), and X-ray diffraction (XRD). HRSEM images were acquired on a LEO 1530 SEM, with accelerating voltage 1–3 kV and working distance between 2 and 7 mm. The reaction product was imaged by SEM on the Si wafer that was placed in the reactor to collect it. HRTEM and EDS were performed on a JEOL 2010F TEM equipped with an Oxford INCA ED spectrometer. Images were acquired using 200 kV accelerating voltage. TEM samples were prepared by drop casting the colloidal product from chloroform dispersions onto carbon-coated TEM grid (Electron Microscopy Sciences). XRD was obtained using a Bruker-Nonius D8 Advanced Θ -2 Θ powder diffractometer with Cu K α radiation ($\lambda = 1.54 \text{ \AA}$), Bruker Sol-X Si(Li) solid-state detector, and a rotating stage. For XRD, the material was drop cast from chloroform onto quartz (0001) substrate. Data were collected for 12–18 h by varying 2 Θ from 20° to 80° in 0.02° increments at a scan rate of 12°/min.

Results and Discussion

Octahedral GeTe Particles. Reactions between DPG and TOP-Te in supercritical hexane at 460 °C and 13.6 MPa

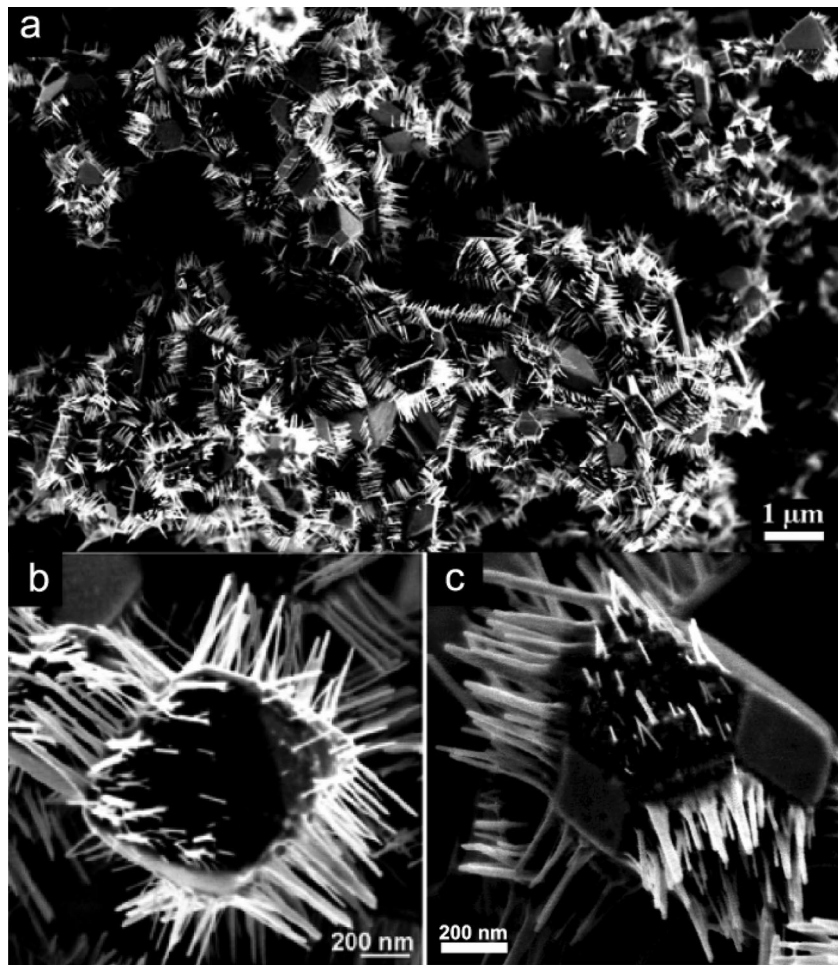


Figure 2. SEM images of colloidal particles obtained from reactions between DPG and TOP-Te in supercritical hexane at 460 °C at 13.6 MPa with 10 vol% octanol. The nanorods are oriented perpendicular to the faceted surfaces of the core particles. In contrast to the octahedral GeTe particles obtained from reactions with octanol, the core particles exhibit a variety of faceted shapes, including truncated octahedra, as in (c) and “irregular” shapes like the particle in (b).

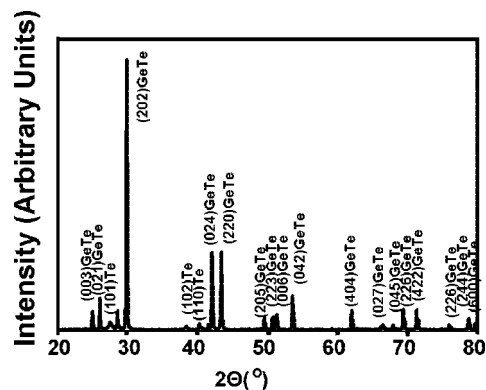


Figure 3. XRD of material obtained from reactions between DPG and TOP-Te in supercritical hexane at 460 °C at 13.6 MPa with 10 vol% octanol, such as in Figure 2. The diffraction pattern indexes to a mixture of rhombohedral GeTe (JCPDS Card No. 47-1079) and hexagonal Te (JCPDS Card No. 36-1452).

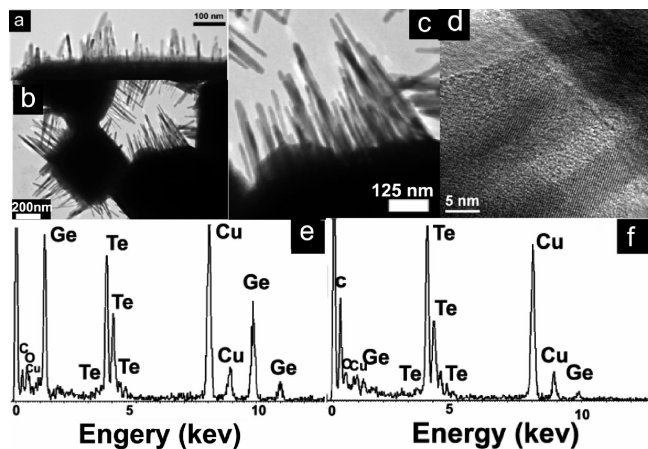


Figure 4. Colloidal particles from reactions between DPG and TOP-Te in supercritical hexane at 460 °C at 13.6 MPa with 10 vol% octanol: (a–d) TEM images and nanobeam EDS data from (e) the core particle and (f) a nanorod. The Ge:Te mole ratios measured in the EDS data were (e) 1:1.1 and (f) 1:20. The C and Cu signals are from the TEM grid.

produced faceted octahedral GeTe particles like those shown in the SEM images in Figure 1. XRD from these particles revealed their composition to be rhombohedral GeTe (JCPDS Card No. 47-1079). This is the room temperature phase of GeTe, which has a rhombohedral unit cell with dimensions of $a = b = c = 5.996 \text{ \AA}$ and $\alpha = 88.18^\circ$. This crystal structure is only slightly distorted from its “high temperature” rocksalt structure with a slight elongation in the $\langle 111 \rangle$ direction.^{64,65} The exposed facets of the octahedral particles are most likely {111} surfaces.

Octanol Addition and Te Nanorod Formation on Faceted GeTe Particles. When octanol was added to the DPG and TOP-Te reactions in supercritical hexane at 460 °C and 13.6 MPa, faceted particles covered with nanorods were produced. Figure 2 shows SEM images of these materials. The nanorods are densely packed and extend perpendicular to the faceted surfaces of the core particles. Furthermore, the faceting of the core particle changes from octahedral to predominantly truncated octahedral, indicating that octanol adsorption to the GeTe surface is changing the crystallization behavior of the core GeTe particle, in addition to promoting Te nanorod formation. XRD (Figure 3) showed that these particles are composed of two different crystalline materials: rhombohedral GeTe (JCPDS Card No. 47-1079) and hexagonal tellurium (*t*-Te) (JCPDS Card No. 36-1452). Nanobeam EDS (Figure 4) obtained separately from the core particles and from the nanorods revealed that the faceted core is composed of rhombohedral GeTe and the nanorods are Te.

Figure 5 shows SEM images of particulate products obtained from reactions with varying amounts of octanol added. In the absence of octanol, very few Te nanorods were present, and the faceted GeTe particles were predominantly octahedral in shape. The addition of octanol into the reaction mixture led to the formation of Te rods on the GeTe particle surfaces, but at octanol concentrations exceeding 20 vol% in the injection solution, Te nanorod growth became inhibited. Ten vol% octanol was found to give the largest density of long Te nanorods on the faceted GeTe particles. The presence of larger concentrations of octanol also led to rougher surfaces on the core GeTe particles. It is interesting to note that some GeTe surfaces were clean and did not support Te deposition.

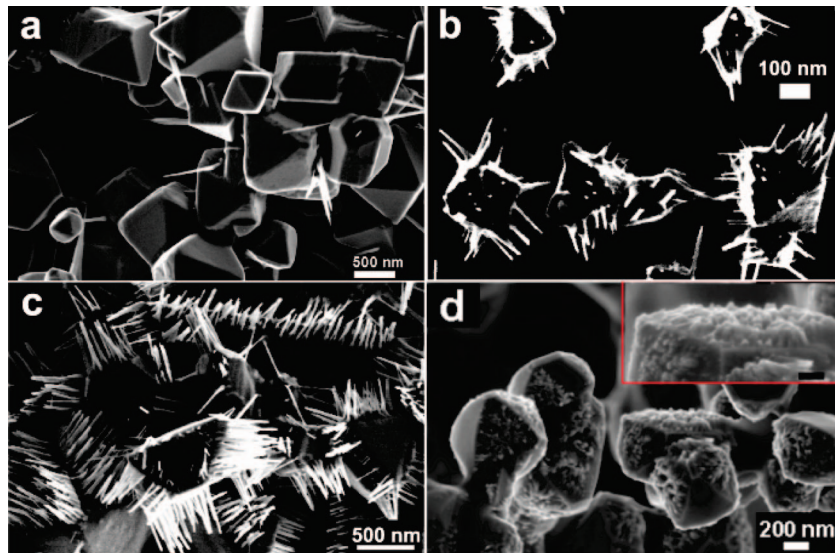


Figure 5. SEM images of the colloidal products obtained from reactions between DPG and TOP-Te in supercritical hexane at 460 °C at 13.6 MPa with varying amounts of octanol added to the injection solution: (a) 0 vol%, (b) 5 vol%, (c) 10 vol%, and (d) 20 vol%.

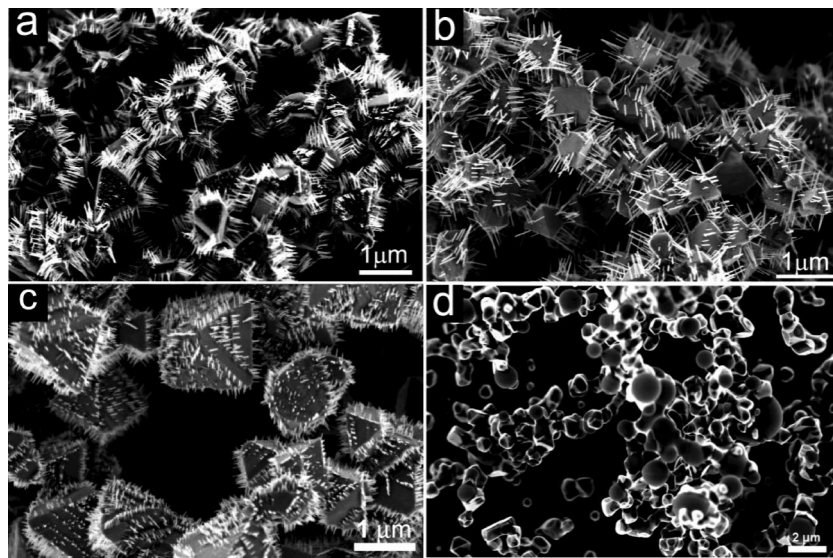


Figure 6. SEM images of colloidal particles produced from reactions of DPG and TOP-Te in supercritical hexane at 460 °C at 13.6 MPa and 10 vol% of (a) octanol, (b) oleic acid, (c) isoprene, and (d) 1-hexadecanethiol in the reaction solution. The Te nanorod diameters and lengths ranged from (a) 5–35 nm and 60–500 nm; (b) 10–60 nm and 30–600 nm; (c) 15–20 nm and 130–150 nm.

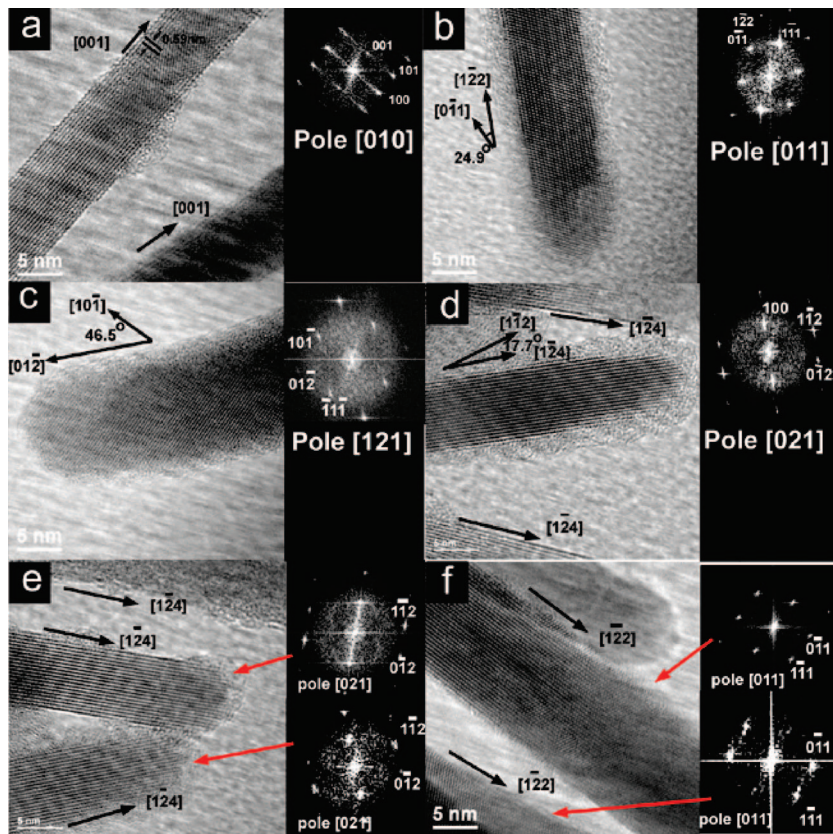


Figure 7. HRTEM images of Te nanorods extended off the GeTe surface. (Insets) Indexed fast Fourier transforms (FFTs) of the imaged nanorods. The indices are given on the basis of a hexagonal unit cell.

The Influence of Other Additives: Oleic Acid, Isoprene, and 1-Hexadecanethiol. The influence of other additives on the morphology of the particles was also tested. Figure 6 shows SEM images of particles produced in the presence of oleic acid, isoprene, and 1-hexadecanethiol. Oleic acid gave rise to structures similar to octanol, but the Te rod density was slightly lower and the diameter distribution was slightly broader. Isoprene also led to the formation of GeTe particles coated with Te nanorods, but the Te nanorods were significantly shorter than

those formed in the presence of octanol or oleic acid and additionally had much sparser coverage on the GeTe surfaces. Hexadecanethiol did not induce Te nanorod formation, and the GeTe core particles did not exhibit distinctly faceted surfaces.

Te Nanorod Crystallography and Growth Mechanism. High resolution TEM images of the Te nanorods (Figure 7) revealed four different growth directions (hexagonal): [001], [12̄2], [012̄], and [12̄4]. The [001] growth direction, i.e., crystallization along

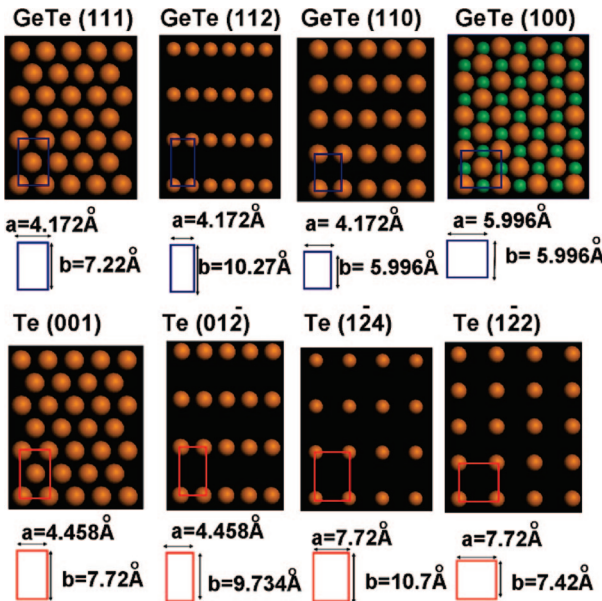


Figure 8. Atomic planes of four GeTe and Te surfaces: (a) GeTe(111), (b) GeTe(112), (c) GeTe(110), (d) GeTe(100), (e) Te(001), (f) Te(01 $\bar{2}$), (g) Te(124), and (h) Te(12 $\bar{2}$). The structures were simulated using the rhombohedral lattice dimensions for GeTe of $a = b = c = 5.995$ Å and $\alpha = 88.18^\circ$, with the $R3m$ (No. 160) space group,⁶⁴ and unit cell dimensions of $4.458 \times 4.458 \times 10.668$ Å³ for hexagonal Te with the $P3_121$ (No. 152) space group.⁶⁹ The green atoms are Ge and the bronze-color atoms are Te.

the crystallographic c -direction, is the commonly observed growth direction for colloidal Te nanorods and nanowires.^{66,67} This is the growth direction that would be expected if the underlying substrate did not influence growth.⁶⁸ The other three growth directions, [124], [01 $\bar{2}$], and [12 $\bar{2}$], are much less likely without intervention from the GeTe surface on the Te nanorod growth direction. It is noteworthy that Te nanorods in the same TEM image—which correspond to aligned nanorods extending off the same GeTe surface facet—have the same growth direction. For example, the nanorods in Figure 7a both exhibit

an [001] growth direction, all six nanorods in Figures 7d and 7e have [124] growth directions, and all three nanorods in Figure 7f have grown in the [122] direction. The faceted surfaces of octahedral GeTe particles formed in the absence of octanol (or other additives) are {111} surfaces. But when octanol, oleic acid, or isoprene was added to the reactions, the GeTe particles were not strictly octahedral and in addition to {111} surfaces, the lower energy {100}, {110}, and {112} surfaces also become exposed. Unfortunately, it was not possible to image directly by TEM the interface between the GeTe surface and the Te nanorod; therefore, the Materials Studio Modeling (MS modeling) software package was used to evaluate which GeTe and Te surfaces are most likely to interface epitaxially with each other by determining the lattice strain between GeTe and Te.

Figure 8 shows simulations of the relevant GeTe and Te surfaces: GeTe(111), GeTe(112), GeTe(110), GeTe(100), Te(001), Te(01 $\bar{2}$), Te(124), and Te(12 $\bar{2}$). Considering both the compatibility between the lattice symmetry and the amount of strain induced at the interface, the most likely pairing of GeTe and Te surfaces are GeTe(111)/Te(001), GeTe(112)/Te(01 $\bar{2}$), GeTe(110)/Te(124), and GeTe(100)/Te(12 $\bar{2}$). Figure 9 illustrates the lattice mismatch at these paired GeTe and Te planes, and the resulting lattice strain is summarized in Table 1. The strain ranges from tensile to compressive, with lattice mismatches from 5.5% to 12%. Even the smallest amount of strain (5.5%) is too large to be sustained with epitaxial deposition of uniform Te layers thicker than a few monolayers on the GeTe surface, and therefore it is not surprising that nanorods grow from the surface. In fact, it appears that it is the strain at the interface that *induces* nanorod growth. The additives (i.e., octanol, oleic acid, and isoprene) must influence the decomposition rates of the Ge and Te reactants, and it appears that Te remains in solution after the Ge reactant has been consumed in the core of the particles, and then the remaining Te deposits on the GeTe surface. Then, although the resulting strain at the GeTe/Te interface cannot be sustained by a uniform coating, it can be accommodated at the interface of the nanometer-size nanowires. Therefore, the wire does not detach during Te growth. The chemical similarity of the GeTe surface and the Te nanowire also aids the adhesion

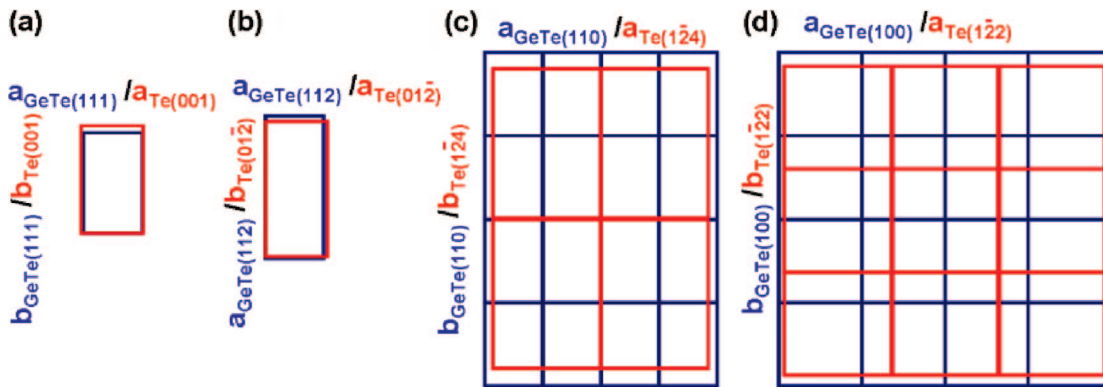


Figure 9. Illustration of the lattice mismatch occurring for four hypothetical GeTe/Te interfaces: (a) GeTe(111)/Te(001), (b) GeTe(112)/Te(01 $\bar{2}$), (c) GeTe(110)/Te(124), and (d) GeTe(100)/Te(12 $\bar{2}$).

Table 1. Atomic Dimensions a and b and the Lattice Strain, δa and δb , at Various Epitaxial GeTe/Te Interfaces

interface	a_{GeTe} (Å)	b_{GeTe} (Å)	a_{Te} (Å)	b_{Te} (Å)	δa (%)	δb (%)
GeTe(111)/Te(001)	4.172	7.22	4.458	7.72	-6.9%	-6.9%
GeTe(112)/Te(01 $\bar{2}$)	4.172	10.72	4.458	9.734	-6.9%	+5.5%
GeTe(110)/Te(124)	4.172	5.996	7.72	10.7	+8.0% ^a	+12.0% ^a
GeTe(100)/Te(12 $\bar{2}$)	5.996	5.996	7.72	7.42	+3.6% ^a	+7.7% ^a

^a Strain between the GeTe(110)-(4 \times 4) and Te(124)-(2 \times 2) surfaces. ^b Strain between the GeTe(100)-(4 \times 4) and Te(12 $\bar{2}$)-(3 \times 3) surfaces.

of the wire to the GeTe core particle. A qualitatively similar effect was observed by Ding, Gao and Wang⁷⁰ at the interface between tin and ZnO nanowires, in which relatively large amounts of strain, up to 12%, could be accommodated at the epitaxial interface between these two materials.

The formation of the GeTe/Te nanorod particles proceeds first by the formation of the core GeTe particles and then Te nanorods grow off their faceted surfaces. It is unclear what mechanistic role octanol and the other additives have in the reaction, but they can modify either reactant decomposition kinetics or passivate or enhance the reactivity of the colloidal particle surface. The data in Figure 5 appear to indicate that the density of Te nuclei increased (i.e., the nanorod coverage was higher) as the octanol concentration increased, corresponding to an enhanced reactivity of the GeTe surface in the presence of octanol. Ten vol% octanol yielded a large number of densely packed Te nanorods on the GeTe particles, and 20 vol% octanol resulted in a nearly continuous, rough layer of Te in which the Te nuclei appear to be nearly fused together. However, it is not certain that octanol enhances nucleation, as 20 vol% octanol also seemed to quench nanorod growth.

Additionally, the other organic additives influenced GeTe particle growth and Te nanorod formation differently. Hexadecanethiol completely quenched nanorod formation and gave rise to GeTe particles that were not faceted. Recently, thiols have been shown to be very effective passivating ligands on Ge surfaces to prevent oxidation,^{60,62} and perhaps the quenching of Te nanorod formation and change in GeTe morphology relates to the Ge–S bonding. Oleic acid gave rise to slightly less nanorod surface coverage than octanol, and isoprene resulted in nanorods that were shorter and thinner with a lower surface coverage. It is also interesting that in the presence of all of the additives, some of the GeTe facets were completely free of Te nanorods. Perhaps the polarity of the surfaces plays a role in this effect. The precise role of the additives appears to be quite complicated and still requires further study.

Conclusion

Reactions between diphenylgermane (DPG) and trioctylphosphine-tellurium (TOP-Te) in supercritical hexane at 460 °C at 13.6 MPa produced colloidal faceted octahedral GeTe particles. When the same reactions were carried out with 10 vol% octanol added, GeTe particles were also obtained, but were coated with Te nanorods. The nanorods extended perpendicular to the faceted GeTe surfaces. The precise role of the octanol (and other additives) is not known, but it can potentially influence reactant decomposition chemistry in solution as well as facet-sensitive surface deposition rates and surface reactions. More study is required to understand the details of how these surfactants lead to these interesting heterostructures.

A careful examination of the crystal structure of the Te nanorods indicated that they grew epitaxially from the GeTe surfaces. The strained interface between GeTe and Te appears to initiate nanorod formation as Te coats the GeTe particles during the reaction. This strain is then accommodated by the nanoscale dimensions of the Te nanorods and they remain attached to the core GeTe particle and formed arrays of aligned Te nanorods. This study provides another indication of how different materials with rather significant lattice mismatch can be epitaxially interfaced at the nanoscale to produce a wide variety of new heterostructure materials with very complicated geometries.

Acknowledgment. This work was financially supported by the Robert A. Welch Foundation, the Advanced Materials

Research Center in collaboration with International SEMATECH, the Advanced Processing and Prototype Center (AP2C: DARPA NR0011-06-1-0005), and the Office of Naval Research (N00014-05-1-0857). We thank J. P. Zhou for TEM assistance.

References

- DeHeer, W. A.; Chatelain, A.; Ugarte, D. *Science* **1995**, *270*, 1179–1180.
- Tzeng, Y.-F.; Liu, K.-H.; Lee, Y.-C.; Lin, S.-J.; Lin, I.-N.; Lee, C.-Y.; Chiu, H.-T. *Nanotechnology* **2007**, *18*, 435703.
- Gangloff, L.; Minoux, E.; Teo, K. B. K.; Vincent, P.; Semet, V. T.; Binh, V. T.; Yang, M. H.; Bu, I. Y. Y.; Lacerda, R. G.; Piro, G.; Schnell, J. P.; Pribat, D.; Hasko, D. G.; Amaralunga, G. A. J.; Milne, W. I.; Legagneux, P. *Nano Lett.* **2004**, *4*, 1575–1579.
- Xue, X. Y.; Li, L. M.; Yu, H. C.; Chen, Y. J.; Wang, Y. G.; Wang, T. H. *Appl. Phys. Lett.* **2006**, *89*, 043118.
- Yang, P.; Yan, H.; Mao, S.; Russo, R.; Johnson, J.; Saykally, R.; Morris, N.; Pham, J.; He, R.; Choi, H.-J. *Adv. Funct. Mater.* **2002**, *12*, 323–331.
- Wu, Y. Y.; Yan, H. Q.; Yang, P. D. *Top. Catal.* **2002**, *19*, 197–202.
- Law, M.; Greene, L. E.; Johnson, J. C.; Saykally, R.; Yang, P. *Nat. Mater.* **2005**, *4*, 455–459.
- Kamins, T. I.; Sharma, S.; Yasseri, A. A.; Li, Z.; Straznicky, J. *Nanotechnology* **2006**, *17*, S291–S297.
- Verplanck, N.; Galopin, E.; Camart, J.-C.; Thomy, V.; Coffinier, Y.; Boukherroub, R. *Nano Lett.* **2007**, *7*, 813–817.
- Wang, Z. L.; Song, J. *Science* **2006**, *312*, 242–245.
- Wang, X.; Song, J.; Liu, J.; Wang, Z. L. *Science* **2007**, *316*, 102–105.
- Henry, T.; Kim, K.; Ren, Z.; Yerino, C.; Han, J.; Tang, H. X. *Nano Lett.* **2007**, *7*, 3315–3319.
- Ng, H. T.; Han, J.; Yamada, T.; Nguyen, P.; Chen, Y. P.; Meyyappan, M. *Nano Lett.* **2004**, *4*, 1247–1252.
- Bryllert, T.; Wernersson, L. E.; Froberg, L. E.; Samuelson, L. *IEEE Electron Device Lett.* **2006**, *27*, 323–325.
- Volkmut, W. D.; Austin, R. H. *Nature* **1992**, *358*, 600–602.
- Kajii, N.; Tezuka, Y.; Takamura, Y.; Ueda, M.; Nishimoto, T.; Nakanishi, H.; Horike, Y.; Baba, Y. *Anal. Chem.* **2004**, *76*, 15–22.
- Seeger, K.; Palmer, R. E. *Appl. Phys. Lett.* **1999**, *74*, 1627–1629.
- Yang, S. M.; Jang, S. G.; Choi, D. G.; Kim, S.; Yu, H. K. *Small* **2006**, *2*, 458–475.
- Hiruma, K.; Yazawa, M.; Katsuyama, T.; Ogawa, K.; Haraguchi, K.; Koguchi, M.; Kakibayashi, H. *J. Appl. Phys.* **1995**, *77*, 447–462.
- Kuykendall, T.; Pauzauskie, P. J.; Zhang, Y.; Goldberger, J.; Sirbuly, D.; Denlinger, J.; Yang, P. *Nat. Mater.* **2004**, *3*, 524–528.
- Islam, M. S.; Sharma, S.; Kamins, T. I.; Williams, R. S. *Nanotechnology* **2004**, *15*, L5–L8.
- Greene, L. E.; Law, M.; Goldberger, J.; Kim, F.; Johnson, J. C.; Zhang, Y.; Saykally, R. J.; Yang, P. *Angew. Chem., Int. Ed.* **2003**, *42*, 3031–3034.
- Ho, S. T.; Chen, K. C.; Chen, H. A.; Lin, H. Y.; Cheng, C. Y.; Lin, H. N. *Chem. Mater.* **2007**, *19*, 4083–4086.
- Bjork, M. T.; Ohlsson, B. J.; Sass, T.; Persson, A. I.; Thelander, C.; Magnusson, M. H.; Deppert, K.; Wallenberg, L. R.; Samuelson, L. *Nano Lett.* **2002**, *2*, 87–89.
- Wu, Y.; Xiang, J.; Yang, C.; Lu, W.; Lieber, C. M. *Nature* **2004**, *430*, 61–65.
- Xiang, J.; Lu, W.; Hu, Y.; Wu, Y.; Yan, H.; Lieber, C. M. *Nature* **2006**, *441*, 489–493.
- Bu, W. B.; Hua, Z.; Chen, H. R.; Shi, J. L. *J. Phys. Chem. B* **2005**, *109*, 14461–14464.
- Lei, B.; Li, C.; Zhang, D. H.; Han, S.; Zhou, C. W. *J. Phys. Chem. B* **2005**, *109*, 18799–18803.
- Manna, L.; Scher, E. C.; Li, L. S.; Alivisatos, A. P. *J. Am. Chem. Soc.* **2002**, *124*, 7136–7145.
- Park, W. I.; Yi, G. C.; Kim, M.; Pennycook, S. J. *Adv. Mater.* **2003**, *15*, 526–529.
- Jung, S. W.; Park, W. I.; Yi, G. C.; Kim, M. *Adv. Mater.* **2003**, *15*, 1358–1361.
- Kuang, Q.; Jiang, Z. Y.; Xie, Z. X.; Lin, S. C.; Lin, Z. W.; Xie, S. Y.; Huang, R. B.; Zheng, L. S. *J. Am. Chem. Soc.* **2005**, *127*, 11777–11784.
- Lauhon, L. J.; Gudiksen, M. S.; Wang, C. L.; Lieber, C. M. *Nature* **2002**, *420*, 57–61.
- Han, S.; Li, C.; Liu, Z. Q.; Lei, B.; Zhang, D. H.; Jin, W.; Liu, X. L.; Tang, T.; Zhou, C. W. *Nano Lett.* **2004**, *4*, 1241–1246.
- Wu, Y. Y.; Fan, R.; Yang, P. D. *Nano Lett.* **2002**, *2*, 83–86.

(36) Hu, J. Q.; Bando, Y.; Liu, Z. W.; Sekiguchi, T.; Golberg, D.; Zhan, J. H. *J. Am. Chem. Soc.* **2003**, *125*, 11306–11313.

(37) Wang, C. R.; Wang, J.; Li, Q.; Yi, G. C. *Adv. Funct. Mater.* **2005**, *15*, 1471–1477.

(38) Lao, J. Y.; Wen, J. G.; Ren, Z. F. *Nano Lett.* **2002**, *2*, 1287–1291.

(39) Bae, S. Y.; Seo, H. W.; Choi, H. C.; Park, J. *J. Phys. Chem. B* **2004**, *108*, 12318–12326.

(40) Jung, Y.; Ko, D. K.; Agarwal, R. *Nano Lett.* **2007**, *7*, 264–268.

(41) Ye, C. H.; Zhang, L. D.; Fang, X. S.; Wang, Y. H.; Yan, P.; Zhao, J. W. *Adv. Mater.* **2004**, *16*, 1019–1023.

(42) Xu, L.; Su, Y.; Li, S.; Chen, Y. Q.; Zhou, Q. T.; Yin, S.; Feng, Y. *J. Phys. Chem. B* **2007**, *111*, 760–766.

(43) Ostermann, R.; Li, D.; Yin, Y. D.; McCann, J. T.; Xia, Y. N. *Nano Lett.* **2006**, *6*, 1297–1302.

(44) Zhang, D. F.; Sun, L. D.; Jia, C. J.; Yan, Z. G.; You, L. P.; Yan, C. H. *J. Am. Chem. Soc.* **2005**, *127*, 13492–13493.

(45) Shen, G. Z.; Chen, D.; Lee, C. J. *J. Phys. Chem. B* **2006**, *110*, 15689–15693.

(46) Yang, H. G.; Zeng, H. C. *J. Am. Chem. Soc.* **2005**, *127*, 270–278.

(47) Milliron, D. J.; Hughes, S. M.; Cui, Y.; Manna, L.; Li, J. B.; Wang, L. W.; Alivisatos, A. P. *Nature* **2004**, *430*, 190–195.

(48) Xiong, S.; Xi, B.; Xu, D.; Wang, C.; Feng, X.; Zhou, H.; Qian, Y. *J. Phys. Chem. C* **2007**, *111*, 16761–16767.

(49) Kanaras, A. G.; Sonnichsen, C.; Liu, H. T.; Alivisatos, A. P. *Nano Lett.* **2005**, *5*, 2164–2167.

(50) Fanfair, D. D.; Korgel, B. A. *Chem. Mater.* **2007**, *19*, 4943–4948.

(51) Hull, K. L.; Grebinski, J. W.; Kosel, T. H.; Kuno, M. *Chem. Mater.* **2005**, *17*, 4416–4425.

(52) Grebinski, J. W.; Hull, K. L.; Zhang, J.; Kosel, T. H.; Kuno, M. *Chem. Mater.* **2004**, *16*, 5260–5272.

(53) Jun, Y.-W.; Seo, J.-W.; Oh, S.-J.; Cheon, J. *Coord. Chem. Rev.* **2005**, *249*, 1766–1775.

(54) Lee, E. P.; Peng, Z. M.; Cate, D. M.; Yang, H.; Campbell, C. T.; Xia, Y. T. *J. Am. Chem. Soc.* **2007**, *129*, 10634–10635.

(55) Moon, G. D.; Jeong, U.; Xia, Y. *Chem. Mater.* **2008**, *20*, 367–369.

(56) Lankhorst, M. H. R.; Ketelaars, B.; Wolters, R. A. M. *Nat. Mater.* **2005**, *4*, 347–352.

(57) Yu, D.; Wu, J. Q.; Gu, Q.; Park, H. K. *J. Am. Chem. Soc.* **2006**, *128*, 8148–8149.

(58) Lee, S.-H.; Ko, D.-K.; Jung, Y.; Agarwal, R. *Appl. Phys. Lett.* **2006**, *89*, 223116.

(59) Meister, S.; Peng, H. L.; McIlwraith, K.; Jarausch, K.; Zhang, X. F.; Cui, Y. *Nano Lett.* **2006**, *6*, 1514–1517.

(60) Hanrath, T.; Korgel, B. A. *J. Am. Chem. Soc.* **2004**, *126*, 15466–15472.

(61) Lu, X.; Ziegler, K. J.; Ghezelbash, A.; Johnston, K. P.; Korgel, B. A. *Nano Lett.* **2004**, *4*, 969–974.

(62) Wang, D. W.; Chang, Y. L.; Liu, Z.; Dai, H. J. *J. Am. Chem. Soc.* **2005**, *127*, 11871–11875.

(63) Tuan, H.-Y.; Lee, D. C.; Korgel, B. A. *Angew. Chem. Int. Ed.* **2006**, *45*, 5184–5187.

(64) Goldak, J.; Barrett, C. S. *J. Chem. Phys.* **1964**, *44*, 3323–3325.

(65) Edwards, A. H.; Pineda, A. C.; Schultz, P. A.; Martin, M. G.; Thompson, A. P.; Hjalmarson, H. P.; Umrigar, C. J. *Phys. Rev. B* **2006**, *73*, 045210.

(66) Mayers, B.; Xia, Y. N. *J. Mater. Chem.* **2002**, *12*, 1875–1881.

(67) Yu, H.; Gibbons, P. C.; Buhro, W. E. *J. Mater. Chem.* **2004**, *14*, 595–602.

(68) This is the case for example with ZnO nanowire arrays grown from solution. ZnO is a hexagonal crystal and the preferred growth direction of ZnO nanowires is in the [001] direction. As Greene, et al.²² showed, for example, regardless of the underlying substrate, when a ZnO is used, the nanowires always grow in the [001] direction away from the substrate.

(69) Inorganic Crystal Structure Database (ICSD): <http://icsdweb.fiz-karlsruhe.de/>.

(70) Ding, Y.; Gao, P. X.; Wang, Z. L. *J. Am. Chem. Soc.* **2004**, *126*, 2066–2072.

CG8002004